Supporting Information For

Nanosheet-Assembled $MoSe_2$ and S-doped $MoSe_{2-x}$ Nanostructures for Superior Lithium Storage Properties and Hydrogen Evolution Reactions

*Yong Yang, Shitong Wang,Jingchao Zhang, Haoyi Li, Zilong Tang, Xun Wang**

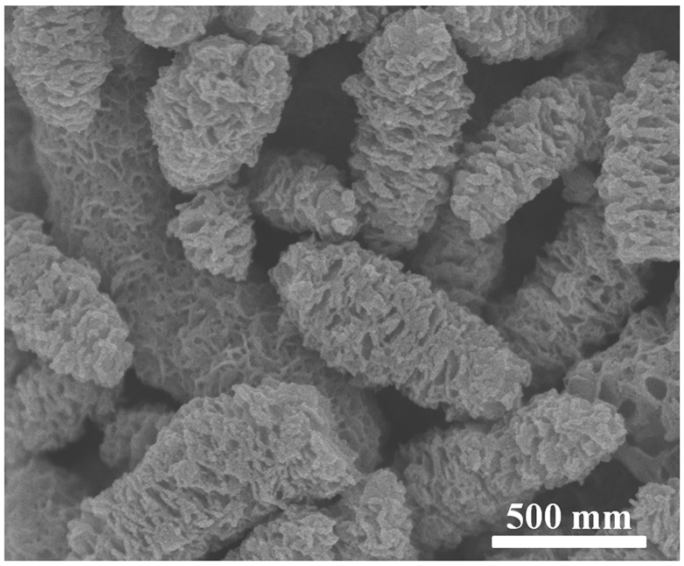

Figure S1. Low-magnification SEM image of as-prepared $MoSe_2$ nanomaterial.

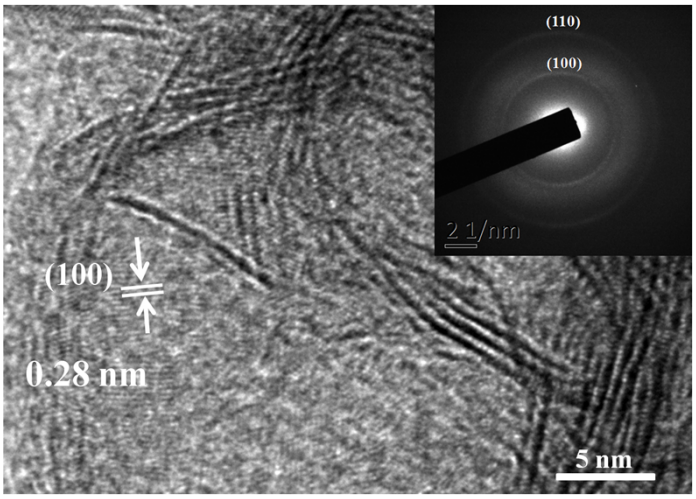

Figure S2. HRTEM image and SAED pattern of $MoSe_2$ nanocaterpillars. The typical SAED pattern shows concentric diffraction rings that can be indexed to the (100) and (110) diffractions of $MoSe_2$, indicating its polycrystalline nature.

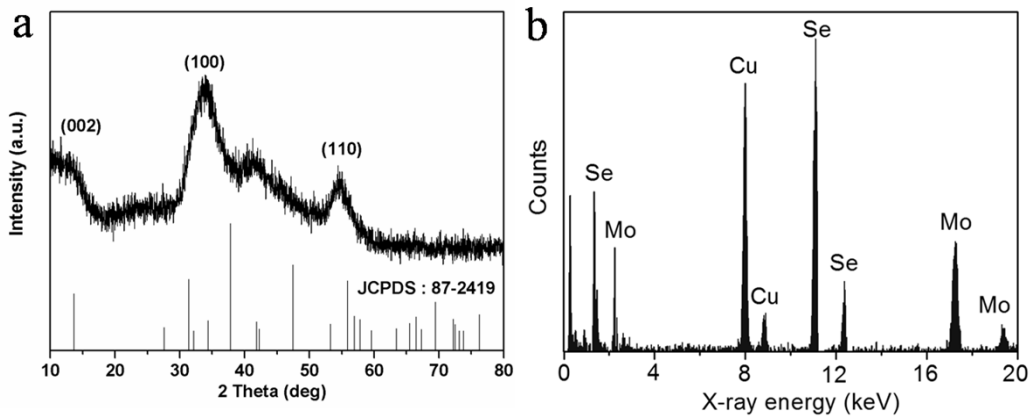

Figure S3. (a) XRD pattern of $MoSe_2$ nanocaterpillars through vacuum drying; (b) Energy-dispersive X-ray spectroscopy spectrums of $MoSe_2$ nanocaterpillars.

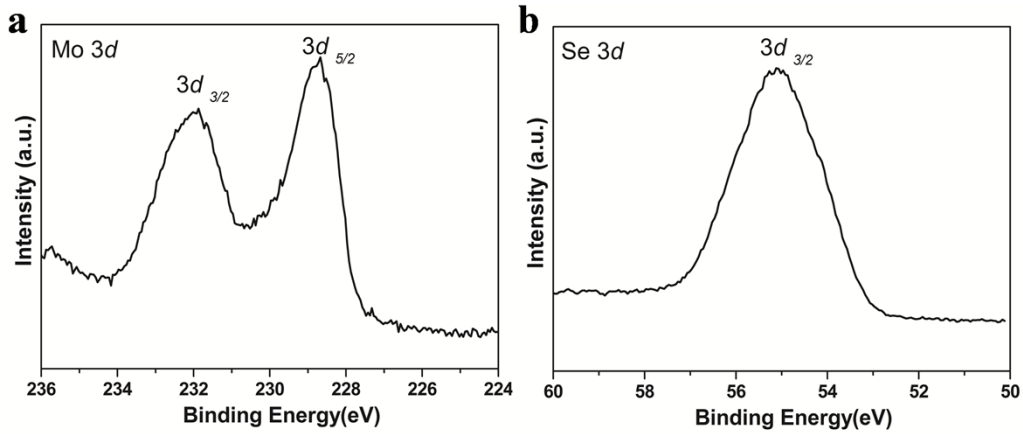

Figure S4. XPS spectra of (a) Mo 3d and (b) S 2p peaks for $MoSe_2$ nanostructures.

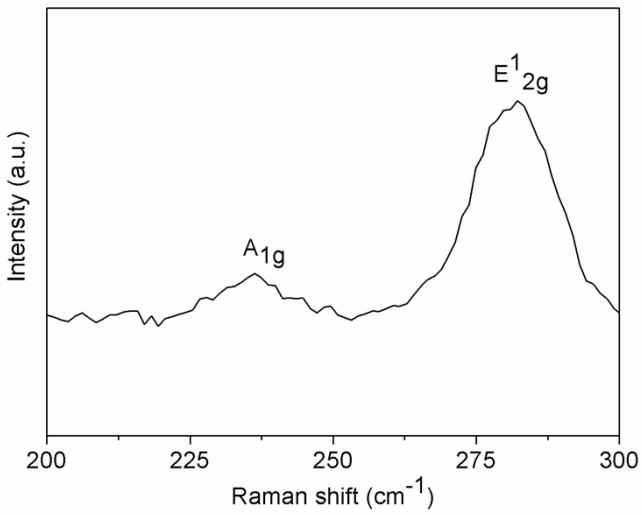

Figure S5. Raman spectrum of $MoSe_2$ nanostructures.

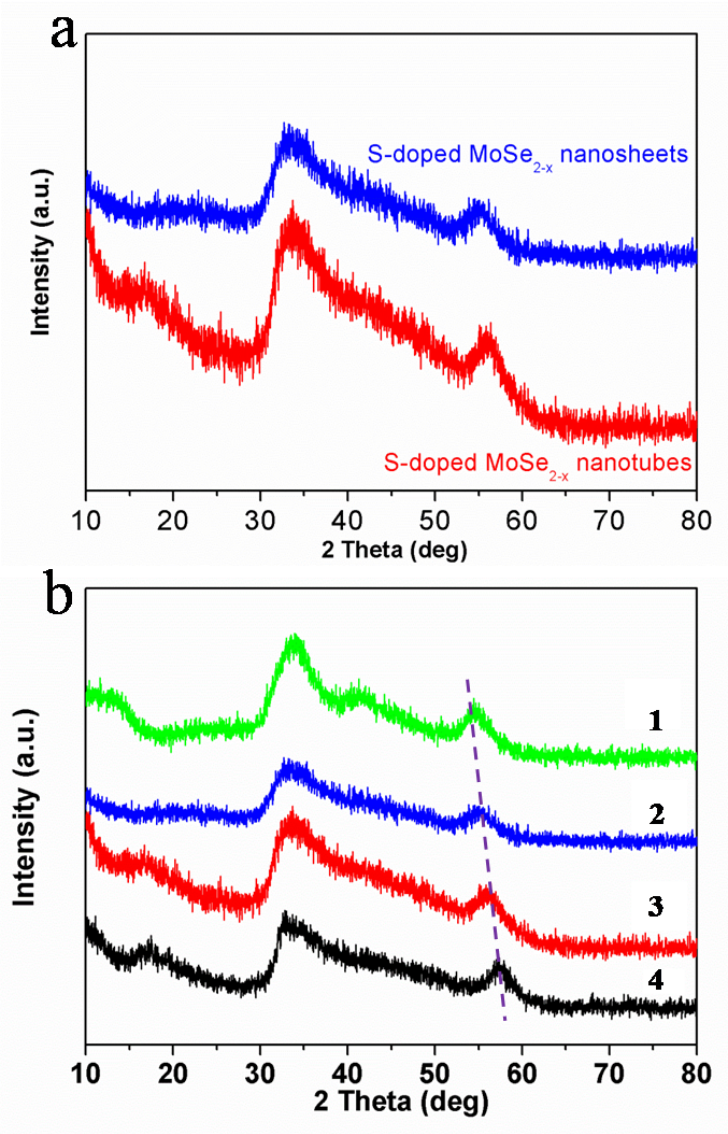

Figure S6. (a) XRD pattern of S-doped $MoSe_{2-x}$ nanosheets and S-doped $MoSe_{2-x}$ nanotubes; (b) XRD pattern of $MoSe_2$ nanocaterpillars (1), S-doped $MoSe_{2-x}$ nanosheets (2), S-doped $MoSe_{2-x}$ nanotubes (3) and MoS_2 (4). As shown in Figure S6b, All peaks of as-prepared MoS_2 can be assigned to MoS_2 phase. It was found that increasing the sulfur content results in a continuous right shift for the diffraction (110) peaks. At the same time, the diffraction peaks at $2\theta = 16^o$ for S-doped $MoSe_{2-x}$ nanotubes can be discernible. Dotted lines are added to facilitate in tracking the shifting of (110) peak.

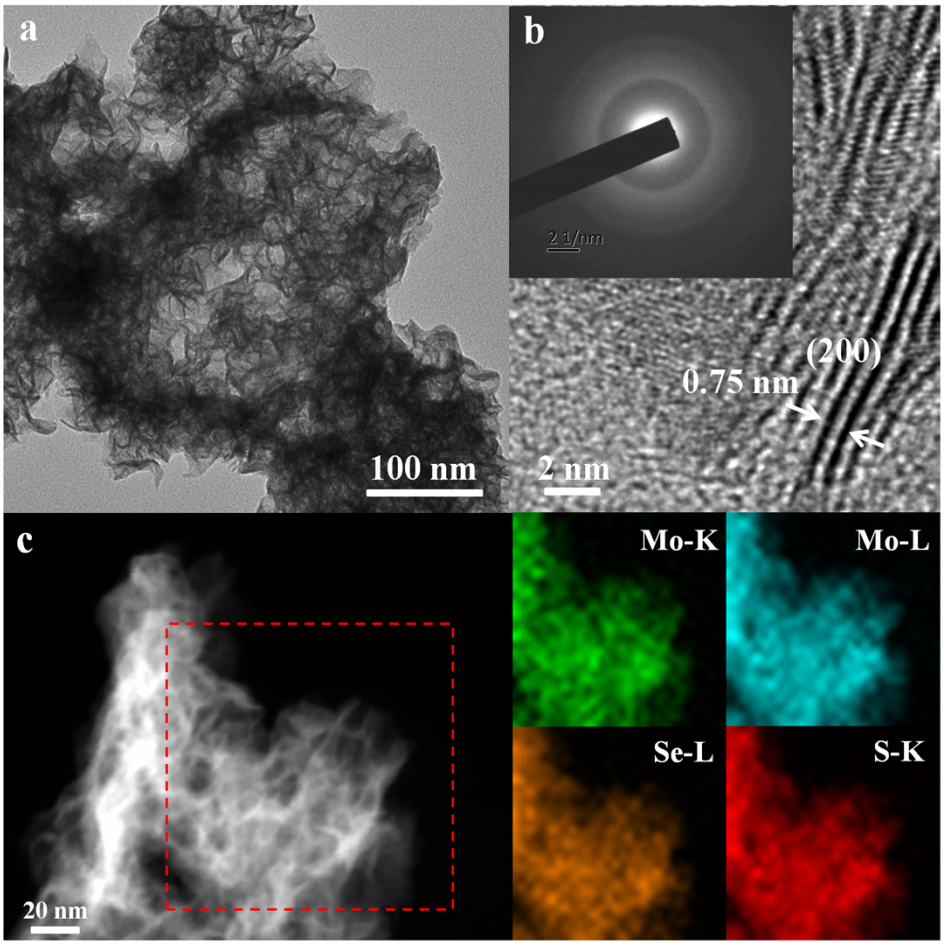

Figure S7. (a-b) TEM images and and SAED pattern of S-doped $MoSe_{2-x}$ nanosheets. (c) HAADF-STEM image and the corresponding EDS mapping images of S-doped $MoSe_{2-x}$ nanosheets, indicating the homogeneous distribution of S, Mo and Se.

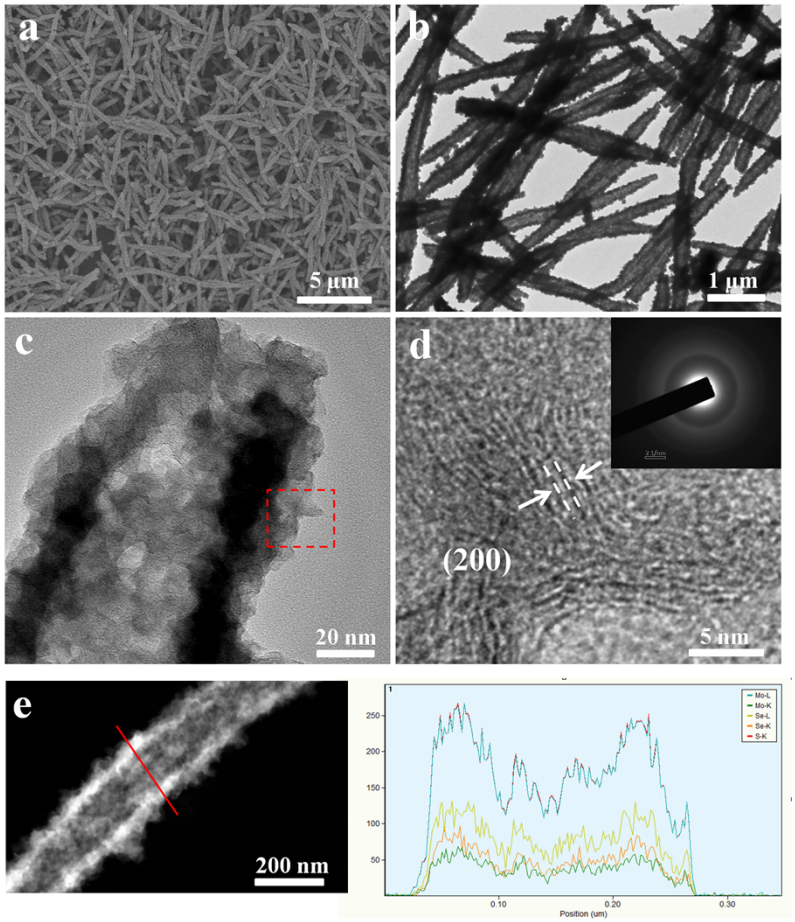

Figure S8. (a-b) Low-magnification SEM image of as-prepared S-doped $MoSe_{2-x}$ nanotubes. (c-d) TEM images and and SAED pattern of S-doped $MoSe_{2-x}$ nanotubes. (e) Corresponding EDS line scan profies.

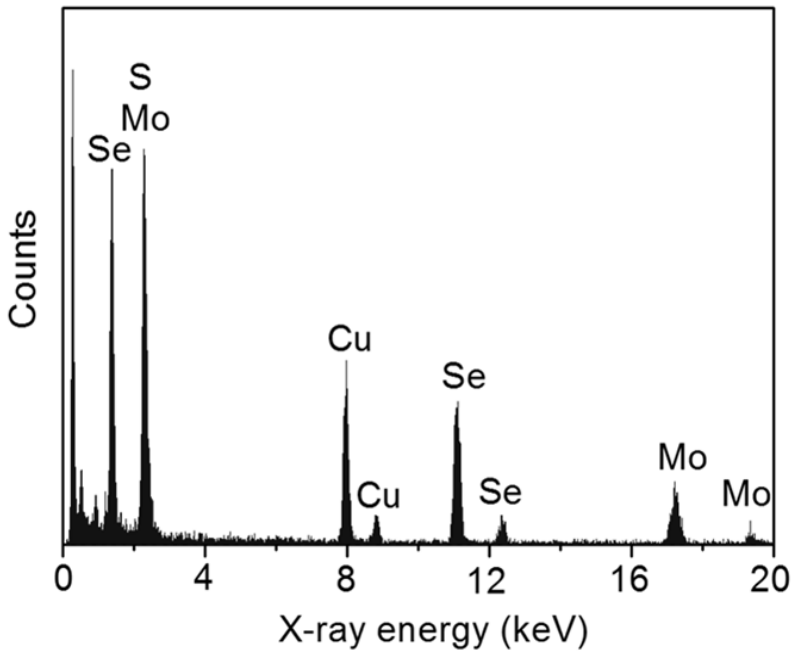

Figure S9. Energy-dispersive X-ray spectroscopy spectrums of as-prepared S-doped $MoSe_{2-x}$ nanotubes.

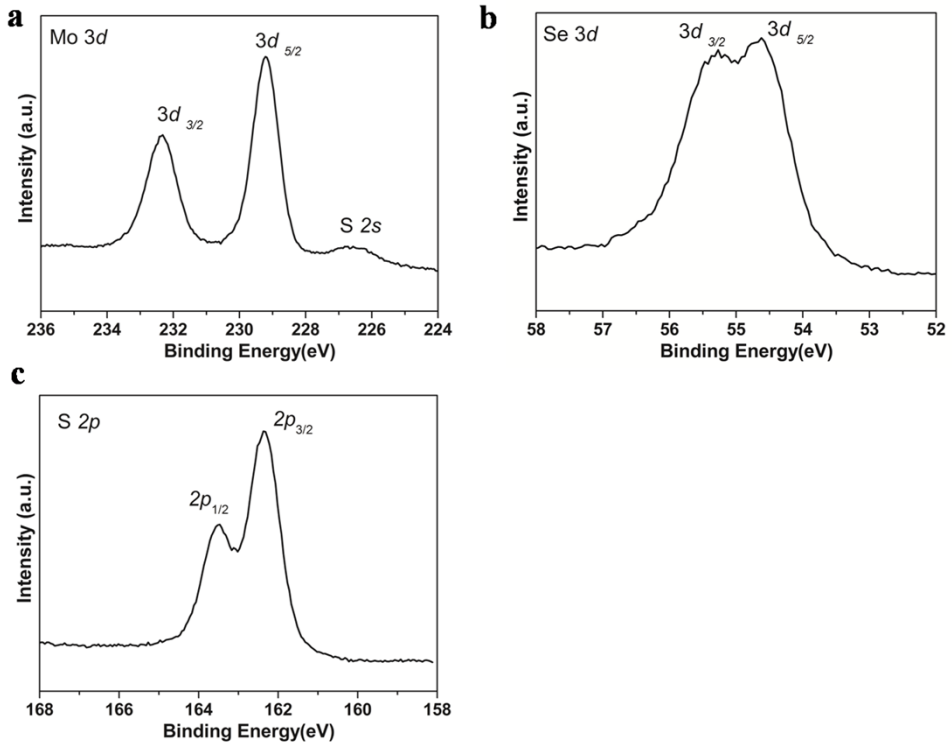

Figure S10. XPS spectra of (a) S 2p peaks, Se 3d (b) and Mo 3d and S 2s peaks (c) for as-prepared S-doped $MoSe_{2-x}$ nanotubes.

Table S1. EDX analysis of the as-prepared samples.

Atomic %	S-doped $MoSe_{2-x}$ nanosheets	S-doped $MoSe_{2-x}$ nanotubes
S (*K*)	11.3	23.2
Mo (*L*)	45	51.5
Se (*K*)	43.7	25.3

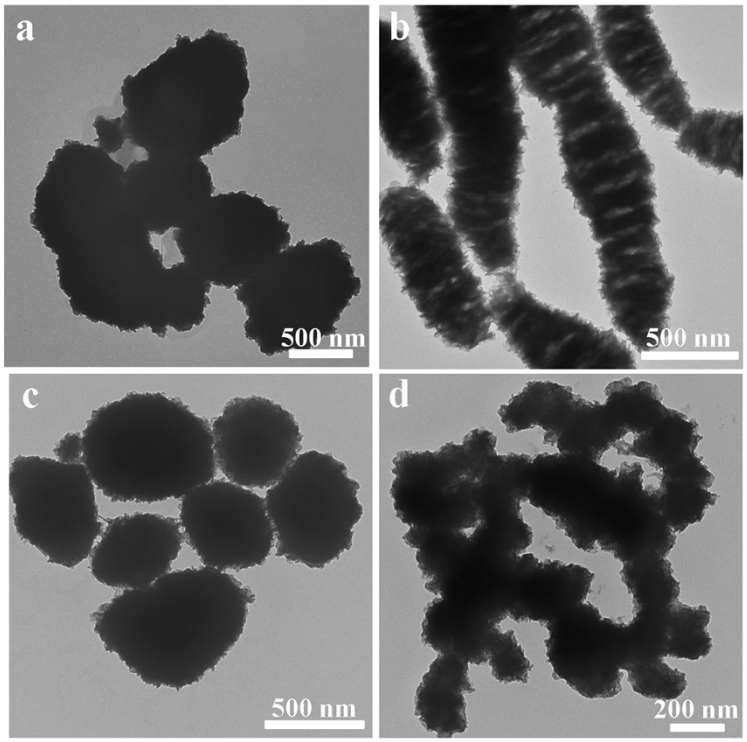

Figure S11. (a) TEM image of the product in pure octylamine system. TEM images of the productes with adding different alcohol：(b) oleyl alcohol；(c) heptyl alcoho；(d) alcohol.

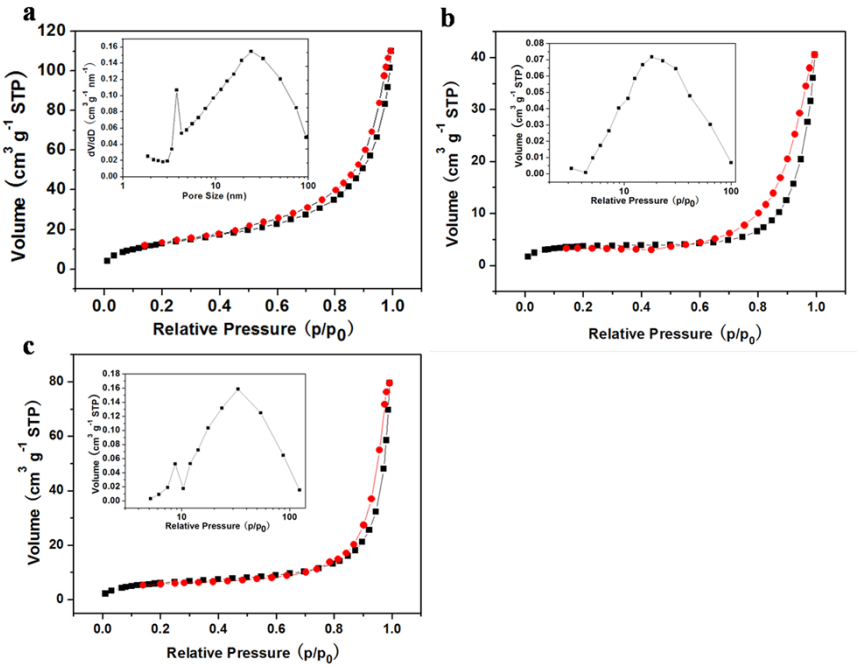

Figure S12. (a) N_2 adsorption/desorption isotherms and the corresponding pore size distribution of S-doped $MoSe_{2-x}$ nanotubes. (b) N_2 adsorption/desorption isotherms and the corresponding pore size distribution of $MoSe_2$ nanocaterpillars. (c) N_2 adsorption/desorption isotherms and the corresponding pore size distribution of S-doped $MoSe_{2-x}$ nanosheets.

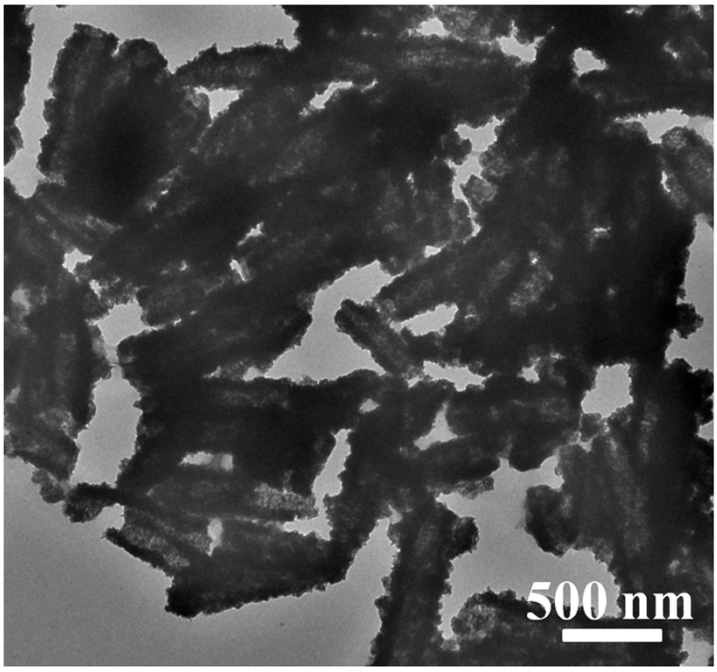

Figure S13. TEM image of S-doped $MoSe_{2-x}$ nanotubes after annealing.

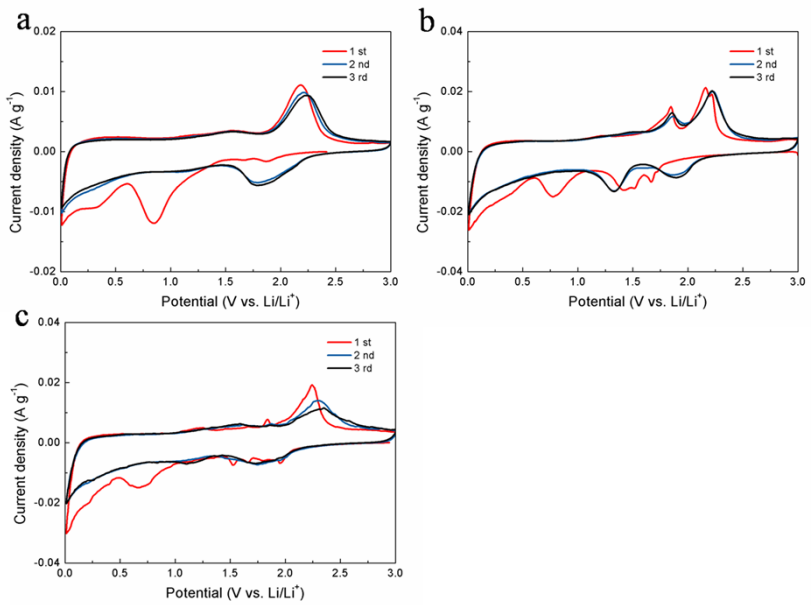

Figure S14. The first three cycles CV curves of all samples at a scan rate of 0.1 mV s^{-1}. S-doped $MoSe_{2-x}$ nanotubes (a), $MoSe_2$ nanocaterpillars (b) and S-doped $MoSe_{2-x}$ nanosheets (c). For $MoSe_2$ nanocaterpillars, the reduction peak at ~0.8 V during the first cycle may be attributed to the formation of Li_xMoSe_2, as shown in Figure S14b. During the following discharge cycles, a strong peak observed at ~0.8 V disappears while two new peaks are repeatedly observed at ~1.3 V and ~1.9 V.

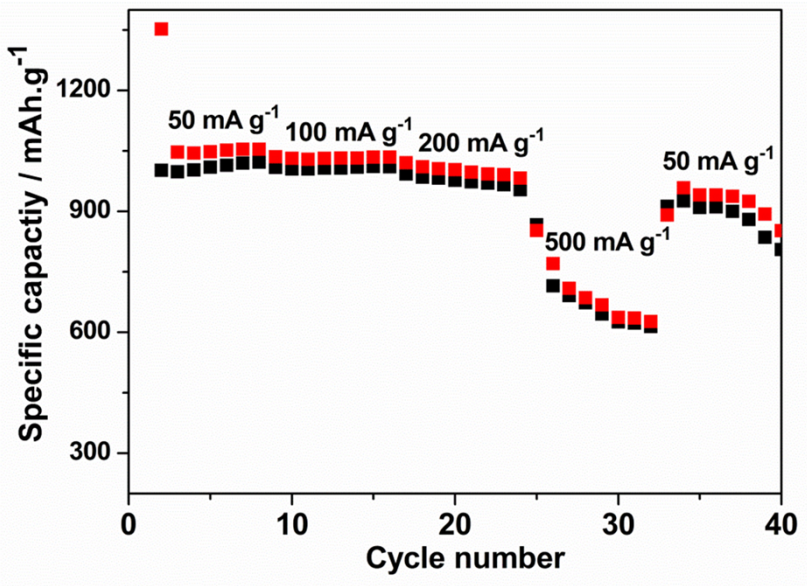

Figure S15. Rate performance of S-doped $MoSe_{2-x}$ nanotubes at various current densities.

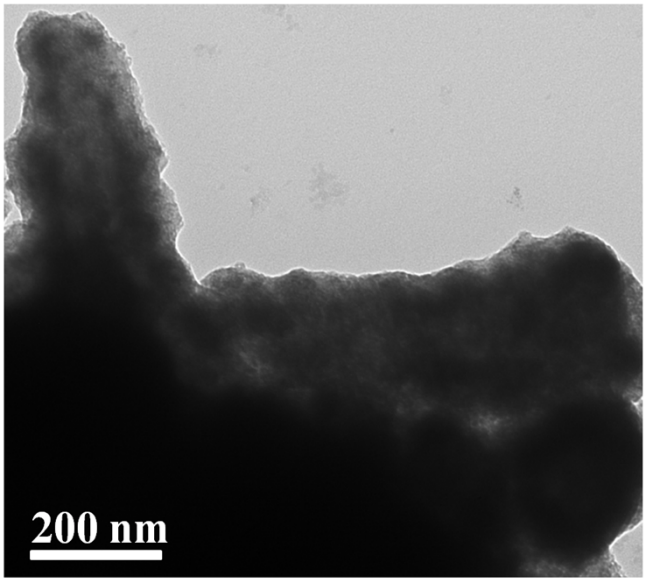

Figure S16.TEM images of the S-doped $MoSe_{2-x}$ nanotubes after cycling for 30 cycles.

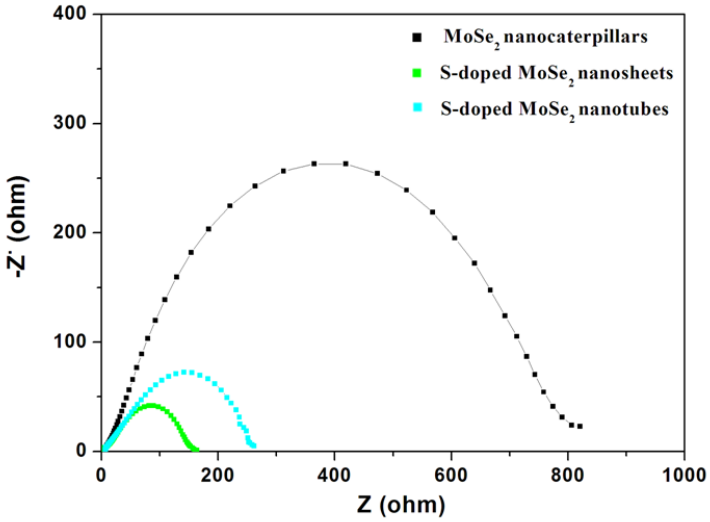

Figure S17. Nyquist plots of $MoSe_2$ nanocaterpillars, S-doped $MoSe_{2-x}$ nanosheets and S-doped $MoSe_{2-x}$ nanotubes.